

Effect of polymer type on the characteristics of ZnO embedded nanocomposite membranes

Bahadır Mert Erdugan^a, Sakhavat Dadashov^a, Elif Demirel^{a,*}, Ender Suvaci^b

^aFaculty of Engineering, Department of Chemical Engineering, Eskisehir Technical University, 26555 Eskisehir, Turkey, Tel. +90 222 321 3550/6509; emails: elifyildiz@eskisehir.edu.tr (E. Demirel), bahadimerterdugan@eskisehir.edu.tr (B.M. Erdugan), sakhavatdadashov@eskisehir.edu.tr (S. Dadashov)

^bFaculty of Engineering, Department of Materials Science and Engineering, Eskisehir Technical University, 26555 Eskisehir, Turkey, Tel. +90 222 321 3550/6356; email: esuvaci@eskisehir.edu.tr

Received 13 April 2020; Accepted 14 October 2020

ABSTRACT

In the present study, ultrafiltration (UF) membranes were manufactured using different polymeric backbone materials such as polyvinyl chloride (PVC) and polysulfone (PSf) and modified with ZnO nanoparticles using a varying ratio of 0.1–2.0 wt.% in order to achieve the best filtration performance. Moreover, compositions of the casting solutions of the pristine membranes in terms of polymer/solvent and polymer/pore-former ratios were varied to determine the best pristine membrane recipe. The results showed that 0.5% ZnO loading provided the highest water flux performance for both PVC and PSf based membranes, which were found as 420 and 426 L/m²h, respectively, under the transmembrane pressure of 0.7 bar. Several characterization techniques were carried out to examine thermal and mechanical properties, as well as morphological structures in comparison to the pristine membranes. The type of polymeric backbone material exhibited a significant effect not only on the filtration performance but also on the lifetime and mechanical properties of the UF membranes. The results clearly indicate that the compatibility of ZnO nanoparticles with PVC is better than PSf under identical fabrication conditions.

Keywords: Membrane; Ultrafiltration; Polymer; Nanoparticle; Zinc oxide; Nanocomposite

1. Introduction

Ultrafiltration (UF) membrane technology has been considered as one of the most important areas in water treatment technologies in recent years. UF technology offers cost-effective and environmentally friendly process with high selectivity and efficient separation of pollutants from water compared to other purification technologies such as chemical and biological treatment processes [1,2]. An effective UF membrane exhibits important features such as high flux, high rejection, low fouling tendency, good mechanical properties, and chemical resistance. Selecting proper membrane materials along with the membrane preparation

technique plays a major role in membrane performance. Organic polymers are the most widely used materials in ultrafiltration membrane fabrication. Although all polymers can be used as a barrier or membrane material, chemical, and physical properties may differ so much that only a limited number can be used as membrane material [3].

The composition of the casting solution along with the specific preparation technique determines the final morphology and hence filtration performance of the membrane [4]. UF membranes can be prepared by using a single polymer or a mixture of two different polymer blends. In practice, frequently used polymeric materials for UF membrane fabrication are polyvinylchloride (PVC), polysulfone (PSf),

* Corresponding author.

polyvinylidene fluoride (PVDF), polyethersulfone (PES), polyacrylonitrile (PAN), and polyethyleneimine (PEI) [5,6]. Among these polymers, PVC based membranes provide excellent chemical properties and high resistance to pH, chemical, temperature, and microbial corrosion with a low material cost, which encourages the growth of production on industrial scale [7]. PSf based membranes exhibit wide pH tolerance, high temperature limit, and good oxidant resistance [8]. Molecular configuration of the polymer in the membrane matrix and functional groups in the polymer chain has significant effects on membrane performance [9]. In general, polymers with low surface energy and high hydrophobicity cause flux decline and irreversible fouling which subsequently reduces the membrane performance and lifetime. PVC based membranes are hydrophobic due to their hydrocarbon chains while PSf based membranes contain hydrophobic aromatic groups in their structure [10,11]. However, membrane fouling remains a major problem, which is usually caused by the deposition of organic pollutants on the membrane surface or adsorption into the membrane pores which increases the operating costs and restricts the practical applications of UF membranes [12].

Several methods have been developed in order to enhance some of the membrane properties including water flux, hydrophilicity, mechanical strength, rejection, and surface formation of membranes [13]. One of these methods is the incorporation of various types of hydrophilic nanoparticle fillers into membrane matrix. Inorganic nanoparticles usually have high surface energy by their nature. Therefore, it makes them highly hydrophilic and very suitable for embedding into the membrane matrix [14]. Inorganic nanoparticles can be categorized as oxide nanomaterials, carbon-based nanomaterials, silicon-based nanomaterials, and metal nanomaterials [2]. Some commonly used metal-oxide nanoparticles are TiO_2 , Al_2O_3 , ZnO , SiO_2 , Fe_2O_3 , and ZrO_2 [15–36].

Incorporation of nanoparticles into membrane structure will result in the formation of weak Van der Waals interactions between functional groups in polymer chain and nanoparticles, which in turn makes the membrane less hydrophobic. There will be two possible outcomes of such an approach. First, during the phase inversion, the exchange rate between solvent and non-solvent will be affected; therefore, pore characteristics of the membranes will be altered [37]. Secondly, during filtration, a water layer between the membrane and foulant molecules will be formed due to the hydrophilic structure. Accordingly, foulant molecules will not be able to contact and stick to membrane surface [38].

Among the nanoparticles used in membrane fabrication, ZnO shows very promising properties, due to having a high surface to volume ratio, high catalytic activity, effective antibacterial, and bactericide capabilities and also lower cost in comparison to other nanoparticles used in the fabrication of nanocomposite membranes. However, studies related to the incorporation of ZnO nanoparticles into membranes are still limited. Rabiee et al. [29] found that embedding ZnO nanoparticles into PVC based membrane matrix significantly increased flux and flux recovery ratio and brought along remarkable changes in pristine membrane morphology. Alhoshan et al. [39] fabricated a mixed matrix membrane consisting of a PSf and ZnO nanoparticles.

They found that incorporation of ZnO nanoparticles into the membrane matrix resulted in a more hydrophilic, smooth, and tightly packed surface, which offered a high flux and an effective permeability barrier. Ahmad et al. [31] embedded ZnO nanoparticles in PES based membranes with *N*-methyl-2-pyrrolidone (NMP)-acetone mixture as solvent. They concluded that improving hydrophilicity encourages pore formation; however, agglomeration of ZnO nanoparticles cannot be avoided with increasing amount of ZnO loading. Leo et al. [27] fabricated PSf based membranes in the presence of ZnO nanoparticles and achieved the highest flux value with 2 wt.% ZnO loading. However, they also observed a tendency of increased agglomeration with increasing ZnO addition. Hong and He [40] studied on the fabrication of ZnO added PVDF membranes and found out that morphological properties, especially mechanical strength of PVDF based membranes significantly enhanced with 1% ZnO addition. They stated that the cross-links formed between ZnO nanoparticles and polymer chains and increase of ZnO loading caused decrease in mechanical strength due to the agglomeration of nanoparticles reducing the flexibility of the polymer chains. Rajabi et al. [41] synthesized PES based membranes using ZnO nanoparticles with two different shapes (equiaxed and nanorod) and concluded that a small amount of nanorod-shaped ZnO was more effective than equiaxed ZnO particles. Javdaneh et al. [42] prepared ZnO/PSf nanocomposite membranes for enhanced antifouling and filtration performance of biological macromolecules. They stated that the best antifouling performance was achieved by a membrane containing 0.5% of ZnO. Yunos et al. [43] studied the effects of different ZnO concentration on the properties of PSf based membranes. They reported that the pure water flux of the pristine membrane increased as ZnO increased up to 1% and tended to decrease with higher loadings. Shen et al. investigated the effect of ZnO addition on thermal properties of ZnO/PES hybrid membranes. They proposed that the addition of ZnO particles improved the thermal stability of the nanocomposite membranes [44]. Zhang et al. [45] manufactured PVDF based nanocomposite membranes with blending ZnO nanoparticles. It has been observed that the nanocomposite membranes have good surface properties and hydrophilic behavior with enhanced filtration performance and high fouling resistance which was attributed to the distribution of ZnO nanoparticles on the surface of the membranes having hydrophilic characteristics.

Although to date, incorporation of ZnO nanoparticles to various matrix phases has been studied, the compatibilities of polymer matrices with ZnO nanoparticle additives from the filtration performance point of view have not been investigated. Therefore, the research objective of this study was to compare and contrast PVC and PSf matrices in the presence of ZnO nanoparticles for ultrafiltration membrane application. Accordingly, to achieve this objective, PVC and PSf based nanocomposite ultrafiltration membranes were fabricated using ZnO nanofillers with varying loading levels. Prior to fabrication of nanocomposite membranes, effects of polymer percentage, and polymer/pore former ratio of the casting solutions which gave the best membrane performances were determined to further apply the recipe in nanocomposite membrane fabrication. Filtration properties of the nanocomposite membranes in

terms of flux, rejection, and antifouling properties as well as morphological structure, thermal, and mechanical properties were investigated in comparison to pristine PVC and PSf membranes. Performance of nanocomposite membranes fabricated using different polymers were discussed considering the interaction of ZnO with either of the polymers and the resulting properties.

2. Experimental

2.1. Materials

Polyvinyl chloride (PVC, high molecular weight, K -value of 69–71) and PSf (average molecular weight of 36,000 Da) were used as main membrane polymers, polyethylene glycol (PEG, molecular weight of 6,000 Da) was used as a pore-forming agent and NMP (99.5% purity) was used as a solvent in the fabrication of membranes. Zinc oxide (ZnO, particle diameter < 100 nm, Sigma-Aldrich, Germany) was used as a filler. Sodium alginate (SA) (Sigma-Aldrich, Germany) and humic acid (HA) (Sigma-Aldrich, Germany) were used as model foulants to represent polysaccharide-like and acidic substances in wastewater, respectively.

2.2. Membrane preparation

PSf and PVC based membranes were prepared using immersion precipitation phase-inversion method. A casting solution, which consisted of polymer (PVC or PSf), pore former (PEG), and solvent (NMP) with different proportions were mixed into a homogenous solution and cast onto a glass plate using an adjustable casting blade (Paul N. Gardner Company Inc., USA) followed by immersing into a coagulation bath containing a nonsolvent (i.e., water) at 25°C, which resulted in a pore formation due to the exchange between solvent and nonsolvent (Fig. 1). Evaporation time between casting and immersion to the coagulation bath was kept as 15 s. The polymer/solvent ratio was changed

between 14 and 22 wt.% whereas the pore former/polymer ratio was applied as 1/2, 1/3, 1/4, and 1/5 (Tables 1 and 2). For the preparation of nanocomposite membranes, certain amounts of ZnO nanoparticles (0.1–2.0 wt.%) were first dispersed in NMP using an ultrasonic bath for about 4 h and the same procedure was followed as in the preparation of pristine membranes. Membranes were kept in fresh distilled water for 24 h to ensure water-soluble components are leached out of the membrane before filtration performance tests. All the membranes were fully dried in a vacuum oven at 50°C for 24 h to remove the moisture content prior to characterization.

The composition of the casting solutions of PVC and PSf based nanocomposite membranes are given in Tables 3 and 4, respectively.

2.2.1. Viscosity measurement

Viscosity of each casting solution (with compositions given in Tables 3 and 4) was measured using a Rotational Viscometer (Fungilab, Smart R, Spain) at room temperature with 50 rpm speed and 60% torque. At least two separate measurements were carried out on each casting solution and the average values are reported.

2.3. Filtration performance tests

Filtration performance of the membranes was tested in terms of pure water flux, SA rejection, HA rejection, and flux recovery ratio. A dead-end UF system (Millipore, USA) was used for the filtration tests. In a typical filtration test, a membrane sample with an effective area of 28.7 cm² was placed in a stirred cell of 200 mL and water was introduced into the cell using a compressed nitrogen gas at a constant transmembrane pressure (TMP) of 0.7 bar. Before filtration tests, membrane samples were compacted at a TMP of 2.1 bar for 30 min in order to rearrange the polymer

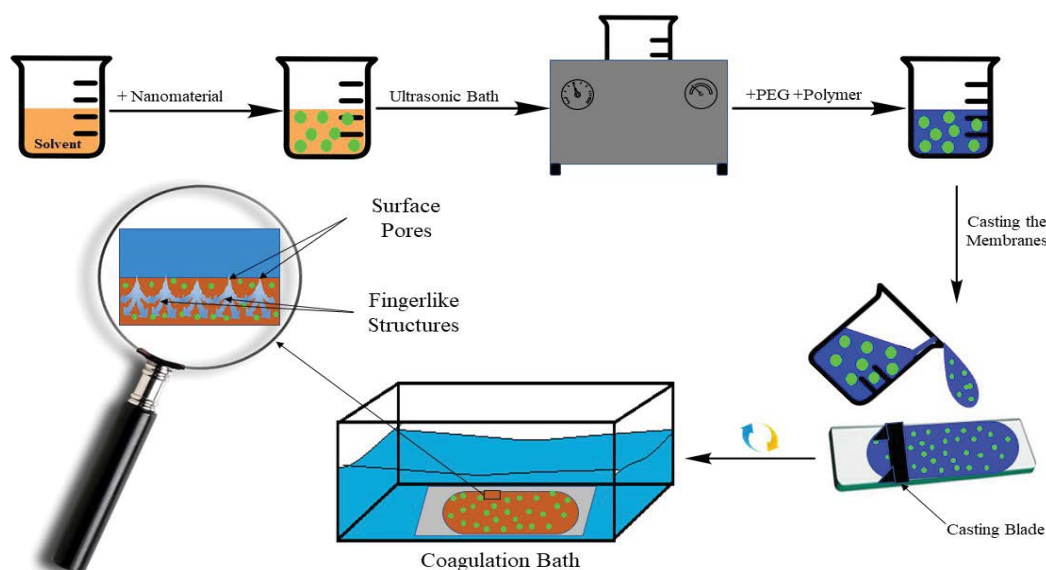


Fig. 1. Schematic view of membrane formation via phase inversion with immersion precipitation technique.

Table 1
Compositions of the casting solutions for pristine PVC membranes with varying ratios

| Polymer (%, wt/wt) | PEG/PVC (wt/wt) | PVC (g) | PEG (g) | NMP (g) | Total (g) |
|-----------------------|--------------------|------------|------------|------------|--------------|
| 14 | 1/4 | 11.2 | 2.8 | 86 | 100 |
| 16 | 1/2 | 10.7 | 5.3 | 84 | 100 |
| 16 | 1/3 | 12.0 | 4.0 | 84 | 100 |
| 16 | 1/4 | 12.8 | 3.2 | 84 | 100 |
| 18 | 1/2 | 12.0 | 6.0 | 82 | 100 |
| 18 | 1/3 | 13.5 | 4.5 | 82 | 100 |
| 18 | 1/4 | 14.4 | 3.6 | 82 | 100 |
| 20 | 1/4 | 16.0 | 4.0 | 80 | 100 |

Table 2
Compositions of the casting solutions for pristine PSf membranes with varying ratios

| Polymer (%, wt/wt) | PEG/PSf (wt/wt) | PSf (g) | PEG (g) | NMP (g) | Total (g) |
|-----------------------|--------------------|------------|------------|------------|--------------|
| 16 | 1/4 | 12.8 | 3.2 | 84 | 100 |
| 18 | 1/4 | 14.4 | 3.6 | 82 | 100 |
| 20 | 1/3 | 15.0 | 5.0 | 80 | 100 |
| 20 | 1/4 | 16.0 | 4.0 | 80 | 100 |
| 20 | 1/5 | 16.7 | 3.3 | 80 | 100 |
| 22 | 1/3 | 16.5 | 5.5 | 78 | 100 |
| 22 | 1/4 | 17.6 | 4.4 | 78 | 100 |
| 22 | 1/5 | 18.3 | 3.7 | 78 | 100 |

Table 3
Compositions of the casting solutions for PVC/ZnO nano-composite membranes (polymer/solvent ratio: 18%, PEG/PVC ratio: 1/3)

| Membrane ID | PVC (g) | PEG (g) | NMP (g) | ZnO (g) | ZnO/PVC (%, w/w) |
|--------------|------------|------------|------------|------------|---------------------|
| Pristine PVC | 13.5 | 4.5 | 82.000 | 0 | 0 |
| PVC/0.25ZnO | 13.5 | 4.5 | 81.966 | 0.03375 | 0.25 |
| PVC/0.50ZnO | 13.5 | 4.5 | 81.932 | 0.06750 | 0.50 |
| PVC/0.75ZnO | 13.5 | 4.5 | 81.899 | 0.10125 | 0.75 |
| PVC/1.00ZnO | 13.5 | 4.5 | 81.865 | 0.13500 | 1.00 |
| PVC/2.00ZnO | 13.5 | 4.5 | 81.730 | 0.27000 | 2.00 |

chains and segments with a lowered volume of porosity and hence to have a stable flux value at the operating TMP. Permeate was weighed in 1 min time intervals and the data was collected using a special software supplied by Radwag (Poland). Water flux values were calculated using the following equation [32]:

$$\text{Water flux } (J_0) = \frac{Q}{A \times \Delta t} \quad (1)$$

Table 4
Compositions of the casting solutions for PSf/ZnO nano-composite membranes (polymer/solvent ratio: 22%, PEG/PSf ratio: 1/3)

| Membrane ID | PSf (g) | PEG (g) | NMP (g) | ZnO (g) | ZnO/PSf (%, w/w) |
|--------------|------------|------------|------------|------------|---------------------|
| Pristine PSf | 16.5 | 5.5 | 78.000 | 0 | 0 |
| PSf/0.10ZnO | 16.5 | 5.5 | 77.9835 | 0.0165 | 0.10 |
| PSf/0.25ZnO | 16.5 | 5.5 | 77.9588 | 0.0413 | 0.25 |
| PSf/0.50ZnO | 16.5 | 5.5 | 77.9175 | 0.0825 | 0.50 |
| PSf/0.75ZnO | 16.5 | 5.5 | 77.8763 | 0.1238 | 0.75 |
| PSf/1.00ZnO | 16.5 | 5.5 | 77.8350 | 0.1650 | 1.00 |

where J_0 is the water flux (L/m^2 h), Q is the volume of the permeate (L), A is the effective membrane area (m^2), and Δt is the time interval for the measurement (h).

After the pure water flux tests, membranes were conditioned using 10 mM NaCl solution for 2 h prior to fouling tests in order to adjust the ionic strength of water [46,47]. Then a solution containing sodium alginate with a pH and concentration of 5.2 and 20 mg/L, respectively, and 10 mM NaCl was fed to the system in order to subject membranes to fouling for 8 h. In the very first 10 min of the fouling test, a permeate sample was taken to calculate the rejection. In order to investigate the humic acid rejection of the prepared membranes, a solution containing 20 mg/L HA was prepared by adjusting the pH of the solution to 10 using 0.1 M NaOH [48]. The collected permeate and feed concentrations of each membrane were determined using a TOC-L analyzer (Shimadzu, Japan). After the determination of total carbon concentrations, the percentage of rejection of each membrane was calculated using the following equation [29]:

$$R(\%) = \left[1 - \frac{C_p}{C_f} \right] \times 100 \quad (2)$$

where C_p and C_f denote the concentrations of the permeate and feed, respectively. At the end of each fouling experiment, membranes were physically cleaned with deionized water and water flux was measured again to calculate flux recovery ratio using the following equation:

$$\text{FRR}(\%) = \left[\frac{J_{w,0}}{J_{w,1}} \right] \times 100 \quad (3)$$

where $J_{w,0}$ and $J_{w,1}$ are the water flux of membranes before and after fouling with SA foulant solution. Resistance in series model, which considers membrane resistance, adsorption resistance, pore plugging resistance, and fouling resistance, has been used in order to better understand the fouling mechanism [49].

$$R_t = R_m + R_r + R_{ir} \quad (4)$$

where R_t is the total resistance during filtration (m^{-1}), R_m is the membrane internal resistance (m^{-1}), R_r is the reversible

membrane resistance (m^{-1}), R_{ir} is the irreversible membrane resistance (m^{-1}).

where R_m and R_t values were calculated by measuring the pure water flux and water flux after fouling membranes with SA solution using the following equations.

$$R_m = \frac{\Delta P}{(\mu \times J_0)} \quad (5)$$

$$R_t = \frac{\Delta P}{(\mu \times J_1)} \quad (6)$$

where ΔP is the TMP (MPa) and μ is the viscosity (Pa s) of the water at the operating temperature. After the backwash cleaning of the membrane, water flux was measured again (J_2) and hence R_r and R_{ir} values were calculated using Eqs. (7) and (8), respectively.

$$R_r = \frac{\Delta P}{(\mu \times J_1)} - \frac{\Delta P}{(\mu \times J_2)} \quad (7)$$

$$R_{ir} = R_t - R_m - R_r \quad (8)$$

2.4. Characterization

2.4.1. Morphological properties

Morphological properties (pore diameter and distribution, porosity, and cross-section images) of the pristine (PVC and PSf based) and ZnO doped nanocomposite membranes were analyzed by scanning electron microscopy (SEM, Hitachi, Regulus 8230, Japan) at an accelerating voltage of 5–10 kV. For surface imaging, samples were coated with gold with a thickness of 2–3 nm (Leica, EM ACE600, Germany) and attached to the carbon strips on the sample holder. For cross-section imaging, samples were immersed in an alcohol and then liquid nitrogen to get them fractured properly.

2.4.2. Porosity, mean pore diameter, and water uptake

Membrane porosity was calculated by the ratio of total pore volume to geometric volume of the membrane [50]. Furthermore, the water uptake value, which provides information about void content and porosity, was determined using the following experimental method. A sample of the membrane having a certain area was kept in water, weighed after carefully wiping the water on the surface and the back of the membrane. The sample was weighed after drying at 60°C in a vacuum oven to evaporate excess water.

Porosity and water uptake values were calculated using the equations below:

$$\varepsilon = \frac{W_{\text{wet}} - W_{\text{dry}}}{\rho_{\text{water}} \times (\pi \times r^2 \times l)} \times 100 \quad (9)$$

$$\text{Water uptake} = \frac{(W_{\text{wet}} - W_{\text{dry}})}{W_{\text{dry}}} \times 100 \quad (10)$$

where ε is the porosity, W_{wet} and W_{dry} are masses of the wet and dry membranes (g), respectively. ρ_{water} is the density of water at 25°C (g/cm^3), r is the radius (cm), and l is the thickness of the membrane (cm).

The overall mean pore diameter values of membranes were determined by Guerout–Elford–Ferry equation by using flux values measured at constant TMP and other membrane properties as given below [51].

$$a = \sqrt{\frac{(2.9 - 1.75\varepsilon) \times (8 \times \mu \times Q_{\text{water}})}{\varepsilon \times A \times \Delta P}} \quad (11)$$

where a denotes overall mean pore diameter (m), ε is porosity, μ is viscosity (Pa s) of the water to be filtered at room temperature, l is the thickness of the membrane (m), Q_{water} is water flux (in m^3/s), A is the surface area of the membrane sample (m^2), and ΔP is TMP (Pa).

Furthermore, surface mean pore size (r) and finger-like pore width of the fabricated membranes were determined using ImageJ software.

2.4.3. Water contact angle

The static water contact angles of the fabricated membranes were measured using a contact angle goniometer (Dataphysics, OCA). A water droplet (50 μL) was applied on different spots of the previously dried membrane sample and the resultant angle was measured. An average of five measurements was reported.

2.4.4. Thermogravimetric analysis

Thermogravimetric analysis was carried out in order to investigate the effect of ZnO addition on thermo-chemical properties of PSf and PVC based pristine membranes. Approximately 10 mg of sample was placed in a platinum pan, which was then heated up to 750°C with a heating rate of 10°C/min using nitrogen as a sweeping gas (30 mL/min). The weight change of the sample was recorded as a function of temperature until the weight of the sample was stabilized.

2.4.5. Mechanical property analysis

To investigate the compressive mechanical performance of the fabricated membranes in terms of surface roughness and Young's modulus, a nanoindentation test was conducted using a nanoindenter (Hysitron, Triboindenter TI 950, USA) utilizing a conical diamond flat punch Berkovich type indenter. The analysis was carried out under a maximum load of 800 μN according to the Oliver–Pharr analysis technique. Based on the measurements, the load displacement curve was obtained and mechanical properties such as hardness and elastic modulus (Young's modulus) of the membrane samples were calculated from the curve. The measurement was carried out on five different spots of each membrane surface and the average of these values was reported.

2.4.6. X-ray diffraction analysis

The crystal structure of the pristine and nanocomposite membranes was determined using an X-ray diffraction

(XRD) instrument (Rigaku, MiniFlex 600 W, Japan) at a scanning range of 2θ : 5° – 100° .

3. Results and discussion

3.1. Water flux and rejection tests for pristine membranes

In order to determine the membrane recipe for the pristine PVC and PSf membranes, polymer/solvent ratio, and PEG/polymer ratio were investigated in terms of water flux and rejection, and the best performing recipe were used for the fabrication of nanocomposite membranes. Fig. 2 demonstrates the effects of polymer/solvent ratio and PEG/polymer ratio on pure water flux and SA rejection of membranes fabricated using different polymers.

According to Fig. 2a, the pure water flux of PVC membrane decreased from 505 to 40 L/m²h, whereas SA rejection increased from 70.6% to 95% with an increase in polymer/solvent ratio from 14% to 20%, which indicated that higher polymer/solvent ratio hinders pore formation [52]. In order to investigate the effect of PEG/PVC ratio, further experiments were carried out at a constant polymer/solvent ratio of 16% and 18% for varying PEG/PVC ratios of 1/4, 1/3, and 1/2. As it can be observed from Fig. 2b, pure water flux increased from 297 to 1,314 L/m²h and SA rejections decreased from 95% to 92% for a constant PVC ratio of 16% when the PEG/PVC ratio was increased from

1/4 to 1/2. In addition, pure water flux increased from 106 to 550 L/m²h, while SA rejections decreased from 94% to 86% for a constant polymer/solvent ratio of 18% when the PEG/PVC ratio was increased from 1/4 to 1/2 (Fig 2c). These results showed that higher amounts of pore former resulted in a more porous structure in the membrane matrix. However, it is well-known that higher pore former ratio and hence higher porosity usually reduce the mechanical strength of the membranes [44,53]. Due to the trade-off between flux and rejection and considering the mechanical strength, an optimum balance of two should be selected. Accordingly, 18% polymer/solvent ratio and 1/3 PEG/PVC ratio was considered to be the most suitable recipe for the casting solution since it gave appreciable values both for flux (350 L/m²h) and rejection (93%).

Furthermore, as it can be shown in Fig. 2d, pure water flux of the PSf based membranes decreased from 782 to 104 L/m²h whereas SA rejections increased from 75% to 98% when the polymer/solvent ratio was increased from 16% to 22%, which can be attributed to the much higher polymer concentration at the interface and a lower porosity resulting in a lower flux [31]. The effect of PEG/PSf ratio was tested at constant polymer/solvent ratios of 20% and 22% since lower polymer concentrations (for 16% and 18%) gave lower rejection values (below 85%). For a constant polymer/solvent ratio of 20%, when the PEG/PSf ratio was reduced from 1/3 to 1/5, a gradual decrease in water

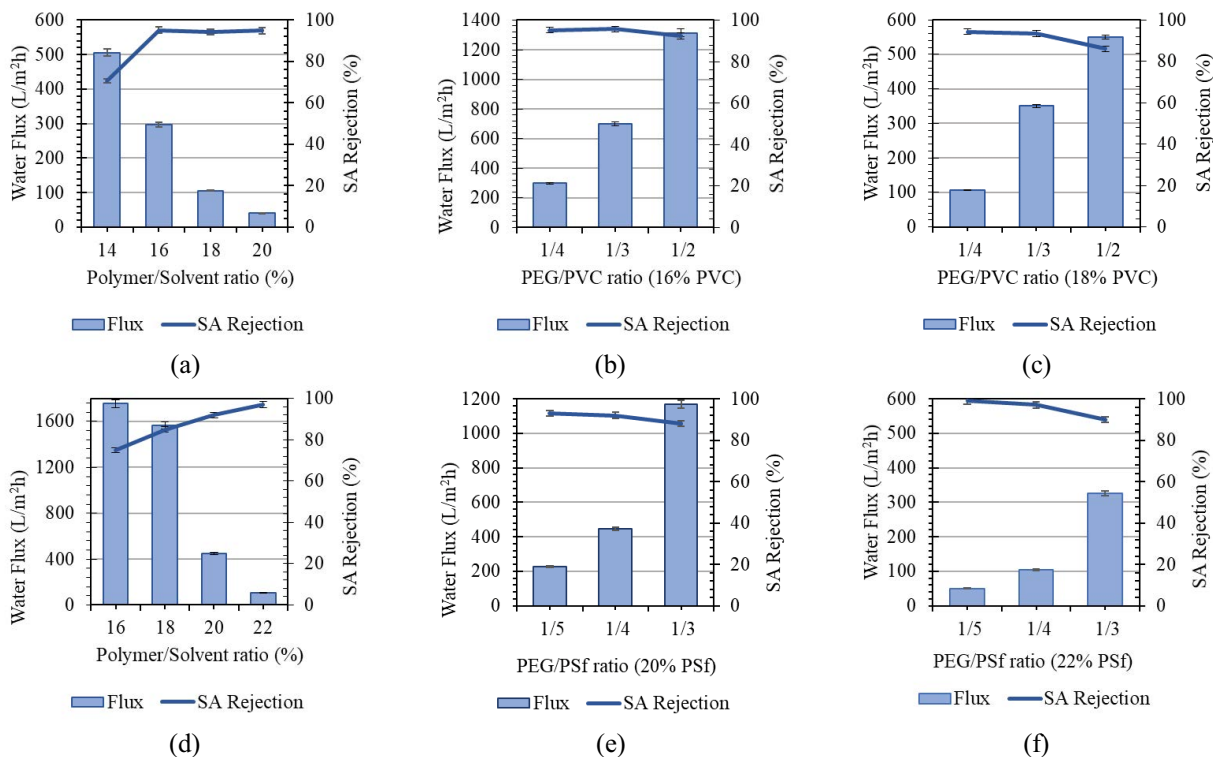


Fig. 2. Effect of (a) polymer/solvent ratio on pure water flux and rejection (PEG/PVC ratio is constant as 1/4), (b) PEG/PVC ratio on pure water flux and rejection (polymer/solvent ratio is constant as 16%), (c) PEG/PVC ratio on pure water flux and rejection (polymer/solvent ratio is constant as 18%), (d) polymer/solvent ratio on pure water flux and rejection (PEG/PSf ratio is constant as 1/4), (e) PEG/PSf ratio on pure water flux and rejection (polymer/solvent ratio is constant as 20%), and (f) PEG/PVC ratio on pure water flux and rejection (polymer/solvent ratio is constant as 22%).

flux was observed and the rejection did not change significantly. Water flux and SA rejection at a PEG/PSf ratio of 1/3 were determined as 520 L/m²h and 88%, respectively. For a constant polymer/solvent ratio of 22%, pure water flux and rejection values were obtained as 326 L/m²h and 90%, respectively. Considering the mechanical strength and hence lifetime of the membrane along with the trade-off between flux and rejection, the most suitable PSf and PEG/PSf ratios were selected as 22% and 1/3, respectively with a water flux of 326 L/m²h and a rejection of 90% to carry out further studies with ZnO nanoparticles [44].

3.2. Water flux and rejection tests for nanocomposite membranes

Fig. 3 demonstrates pure water flux and rejection values of PVC and PSf membranes as a function of ZnO loading levels.

Fig. 3a shows that water flux of pristine PVC membrane increased from 350 to 420 L/m²h (20% increase) when 0.5% ZnO was added into the casting solution. As shown in Fig. 3b, SA and HA rejection of pristine PVC membranes were 93.2% and 82.3%, respectively, and with the addition of ZnO, SA and HA rejections increased to 98.0% (with 0.5% ZnO loading) and 89.4% (with 0.75% ZnO loading), respectively.

The same trend in water flux was observed with PSf based membranes. The flux value was improved by 23.5% (from 326 to 426 L/m²h) while SA rejection increased from 90% to 92% and HA rejection increased from 96.3% to 98.7% with addition of 0.5 wt.% ZnO (Fig. 3b). The increase in flux may be due to the combined effects of porosity,

change in the pore structures, and improvement in hydrophilicity of the polymeric matrices due to the presence of hydrophilic ZnO, which enhanced the phase separation and resulted in bigger pore size, hence a higher water flux [31,39]. Water flux and rejection values tended to decrease beyond 0.5 wt.% ZnO addition both for PVC and PSf based nanocomposite membranes due to the increase in the viscosity of the casting solutions (Fig. 4), thereby delaying the interchange between the solvent and nonsolvent resulting in smaller pore sizes hence lower pure water flux values. In addition, high loadings of ZnO nanoparticles tend to agglomerate due to strong Van der Waals interactions between them, causing membrane surface pores to clog and reduce the flux as also reported earlier by Choi et al. [54].

The dynamic viscosities of casting solutions have been given in Fig. 4 as a function of ZnO loading. As it can be observed from Fig. 4a, the viscosity of PVC based membrane casting solution increased gradually from 2,175 to 2,504 cP with the increasing amount of ZnO nanoparticles added into the solutions. A similar trend was also observed for the PSf based casting solutions, that is, the viscosity of the casting solution for the pristine membrane was 581 cP and it gradually increased up to 641 cP when 1% by wt. ZnO was added.

3.3. Antifouling properties of nanocomposite membranes

In addition to the water flux and rejection properties of the prepared membranes, the resistance of the pores to clogging or fouling without chemical cleaning after exposure to the contaminant solution is also very important.

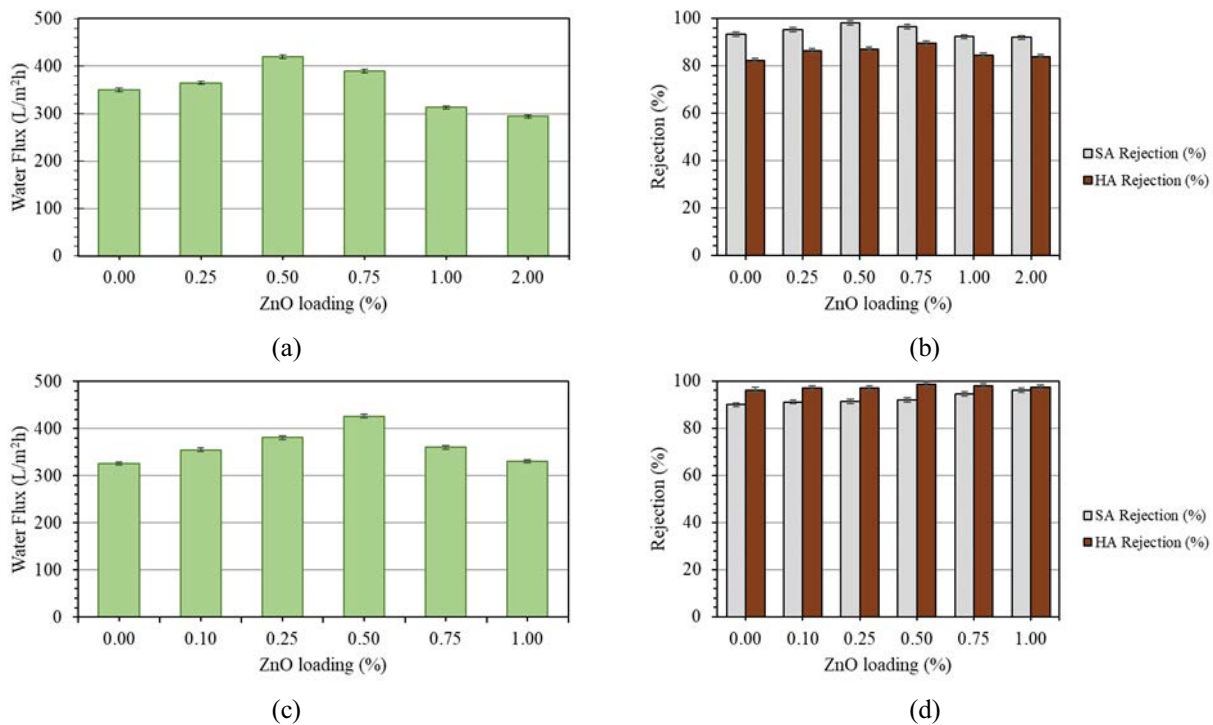


Fig. 3. (a) Water flux, (b) rejection values of PVC based, (c) water flux, and (d) rejection values of PSf nanocomposite membranes as a function of ZnO loading levels.

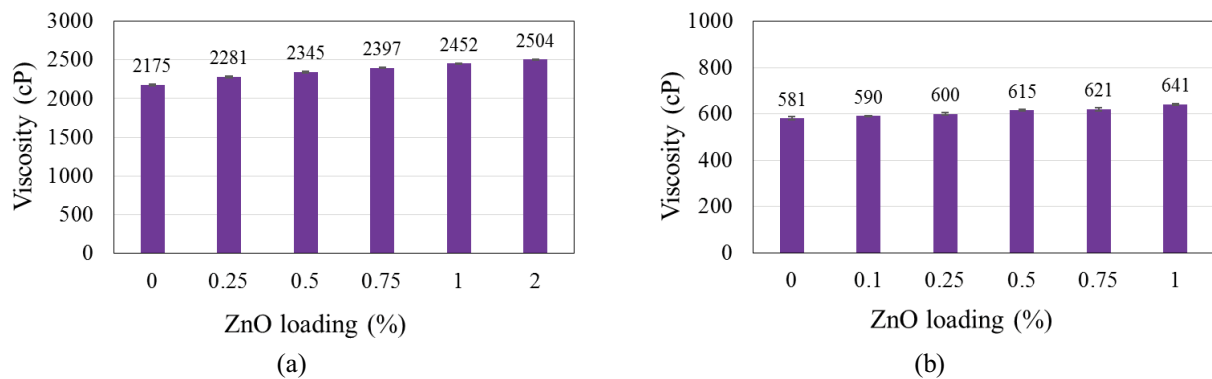


Fig. 4. Dynamic viscosity of (a) PVC based and (b) PSf based pristine and nanocomposite membranes as a function of ZnO loading.

Anti-fouling properties of the pristine and nanocomposite membranes were determined in terms of flux recovery ratio and individual resistances.

Fig. 5 shows integrated flux profile of PVC and PSf based pristine and ZnO doped nanocomposite membranes starting from the measurement of pure water flux, exposure of the membrane to the foulant solution and measuring the pure water flux again after cleaning and backwashing steps. Permeation results indicate that in all steps, they follow a similar trend, that is, starting with higher flux and becoming

steady after a period of time. Pure water flux is higher than SA flux values in all cases (region I). Solution containing SA is less permeable than pure water and the flux tends to decrease with time due to the concentration polarization and cake layer formed on the membrane surface which further leads to adsorption of contaminant particles on the surface and inside the channels (region II) resulting in reduced flux and increased resistance. The recovery of flux after SA fouling test (region III) especially in the case of PVC based nanocomposite membranes has been substantially (90.2% for

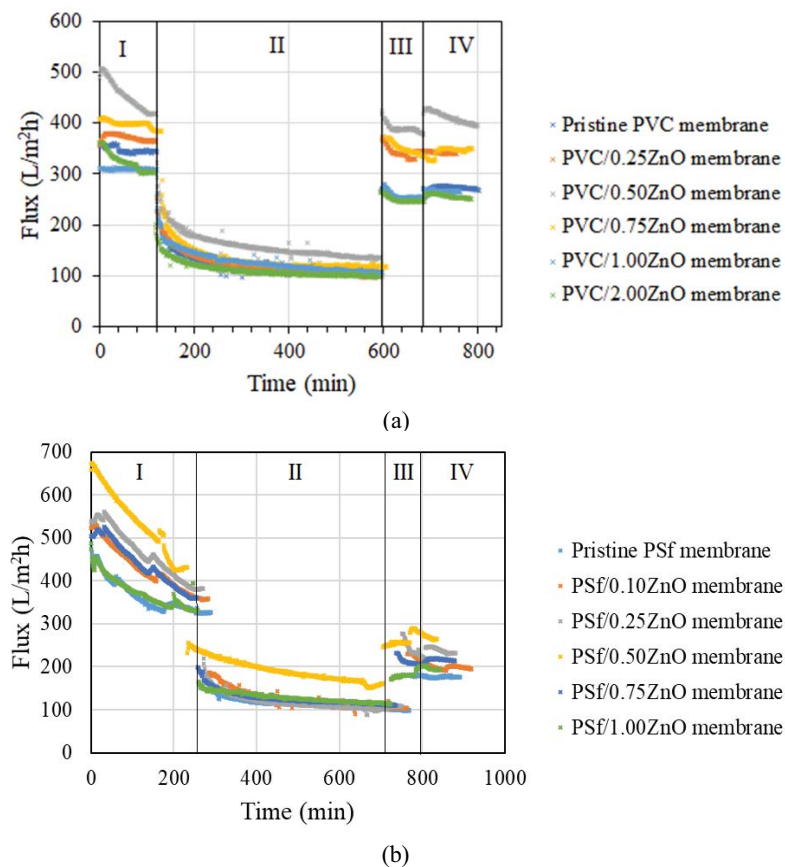


Fig. 5. Integrated flux profiles of (a) PVC based, (b) PSf based pristine and nanocomposite membranes (region I = measurement of pure water flux, region II = flux of SA filtration, region III = flux after SA fouling test, and region IV = flux after backwashing).

PVC/0.50ZnO membrane) increased and a small improvement can be observed after backwashing (region IV). The recovery of flux after physical cleaning and backwashing was not enhanced considerably for PSf based membranes, which exhibit low anti-fouling characteristics as well as high resistance behavior (Fig. 5).

Flux recovery ratio and resistance values for both polymeric based membranes as a function of ZnO loadings are given in Figs. 6 and 7, respectively.

According to Fig. 6a, FRR of pristine PVC membrane was 73.6% and it was improved by almost 22% (90.2%) with the addition of 0.5 wt.% ZnO. The increase in flux recovery ratio by the incorporation of ZnO into the membrane matrix can be attributed to the reduction of the interaction between the contaminant and the membrane surface due to the hydrophilic ends of the ZnO nanoparticles. Further addition of ZnO nanoparticles beyond 0.5% caused FRR value to decrease probably due to agglomeration of nanoparticles on the surface and throughout the finger-like structure as also stated by Yang et al. [55].

FRR value of PSf based pristine membrane was 53.7% and gradually increased to 59.9% with the addition of ZnO into the membrane casting solution (Fig. 6b). The lower flux recovery ratios of both pristine and ZnO doped nanocomposite membranes indicated that the foulant molecules blocked the surface as well as finger-like pores after 8 h of fouling tests, which could not be recovered with physical cleaning. In addition, the slight improvement in flux recovery ratio by the addition of ZnO to pristine PSf membranes shows that intermolecular interactions between ZnO and PSf polymer chains are weaker than those between ZnO and PVC.

In order to better understand and quantify anti-fouling properties of fabricated membranes, resistances of PVC and

PSf based pristine and nanocomposite membranes in terms of R_p , R_m , R_r , and R_{ir} were investigated and the results are presented in Fig. 7.

In Fig. 7, R_m shows the internal or hydraulic membrane resistance, which can be removed by simple hydraulic cleaning and shows poor bonding of the foulant to the membrane surface (cake layer), R_{ir} represents irreversible membrane resistance, which shows clogging of membrane surface and finger-like pores due to contaminant molecules and R_t indicates total membrane resistance [56]. As shown in Fig. 7a, the resistance of the pure PVC membrane gradually decreased with the addition of ZnO and the lowest resistance values were achieved in the presence of 0.5% ZnO loading. This may be attributed to the increased hydrophilicity that decreased the interaction between foulants and membrane, which in turn inhibited the adsorption of foulant molecules onto membrane pores. In other words, PVC membranes could be cleaned by simple hydraulic cleaning as stated by Maximous et al. [23]. Further addition of ZnO led to an increase in resistance values probably due to non-homogeneous distribution of ZnO on the surface as well as throughout the membrane cross-section, which weakened the interaction of ZnO and polymer.

The resistances of the PSf based membranes decreased with the addition of ZnO into the membrane structure and the lowest resistance values were reached in the case of 0.5% ZnO loading. However, due to the weak interaction between PSf and ZnO, resistance of the pristine membrane has not been improved sufficiently. This is also clearly observed from the large difference between irreversible and reversible resistance values in Fig. 7b. Therefore, PSf based membranes have higher fouling tendency than PVC

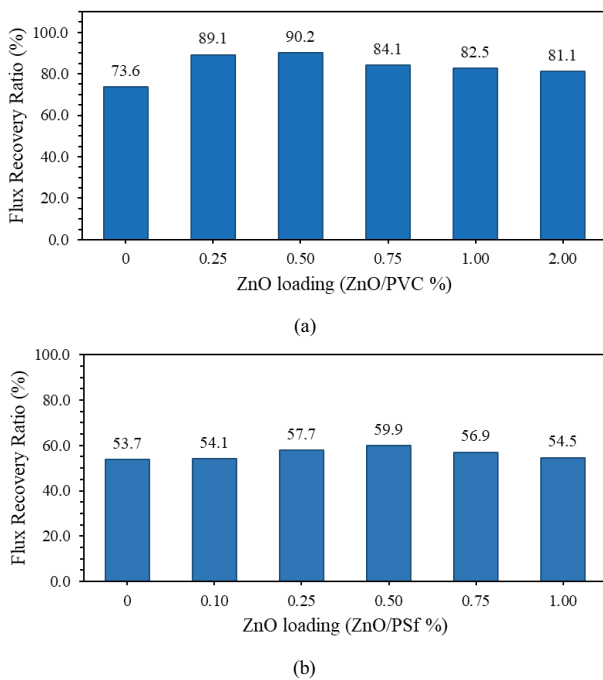


Fig. 6. Flux recovery ratio of (a) PVC based and (b) PSf based membranes as a function of ZnO loading.

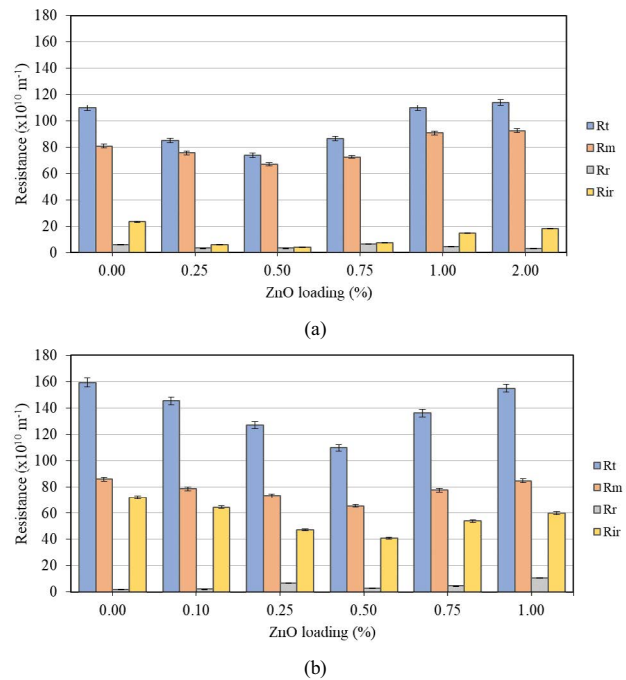


Fig. 7. Resistance values of (a) PVC based and (b) PSf based membranes as a function of ZnO loading.

based membranes. The hydrophilic-hydrophobic properties of the membrane surface have a significant effect on the antifouling property and permeability. The reason for reduced membrane permeability after fouling is that pollutant molecules can adsorb onto the membrane surface and clog the channels. Membranes with hydrophobic surface enable organic pollutants to diffuse more rapidly and cause more pores to block after pollution [57]. This behavior can be attributed to having different chain structures of the polymers. PSf polymer chains are more hydrophobic compared to PVC chains due to the presence of aromatic groups [24]. This nature of PSf, will cause organic pollutants to diffuse more easily into the active layer and form Van Der Waals (hydrogen) bonds between the pollutant molecules and polymer chains. This is why the FRR value of the pristine PSf membrane is much lower compared to that of pristine PVC membrane. The addition of ZnO nanoparticles into the membrane matrix caused high surface hydrophilicity so organic pollutants cannot diffuse onto the membrane surface due to the hydrogen bonds formed between the water molecules and the polymer on the hydrophilic membrane surface [58]. Fig. 8 represents an illustration of the interaction of foulant molecules with a pristine membrane and PVC and PSf based nanocomposite membranes during fouling experiment. The scheme shows that the pollutant molecules form a cake layer on the pristine membrane surface (Fig. 8a) [59,60]. For PVC based membrane, after the addition of ZnO nanoparticles, the membrane surface hydrophilicity increases, and a water layer forms on the surface. Therefore, most of the organic foulant molecules cannot diffuse directly onto the membrane surface and also into the finger-like pores (Fig. 8b) [61]. However, due to the weak interaction between ZnO and PSf chain, most of the ZnO nanoparticles do not remain on the surface but precipitate onto the bottom of the membrane matrix during phase inversion process, hindering the hydrophilic property of the surface, which in turn becomes more susceptible to fouling [11]. This is also confirmed by the contact angle values of the pristine and nanocomposite membranes. The contact angle value of pristine PVC membrane decreased from 64.5° to 38.5° with the addition of 0.5 wt.% ZnO, whereas that of pristine PSf membrane decreased from 68.7° to 57° with the addition of 0.5 wt.% ZnO nanoparticles, which means that ZnO nanoparticles could not be well-incorporated onto the PSf surface.

The interaction of ZnO with either of the polymer chains can be explained by the proposed schematic given

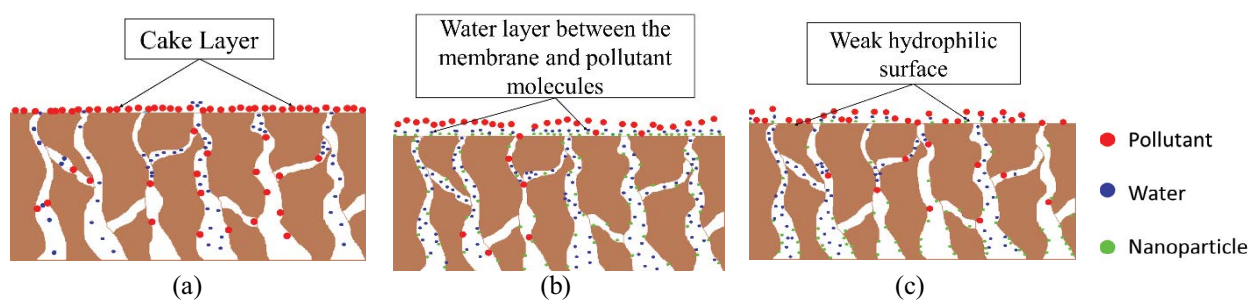


Fig. 8. Schematic image of pristine and nanoparticle added membrane morphologies after SA fouling (a) pristine membrane, (b) PVC based, and (c) PSf based nanocomposite membranes.

in Fig. 9. According to Fig. 9a, PVC chain has more polar characteristics compared to the PSf chain due to the presence of Cl atoms. Therefore, PVC chains with a definite length tend to have a more effective interaction with ZnO nanoparticles than a PSf chain with the same length (Fig. 9b). Due to the strong interaction of ZnO and PVC chain, the amount of ZnO nanoparticles uniformly distributed over the surface of the membrane will be higher, which in turn helps to enhance the surface antifouling properties as also illustrated in Figs. 6 and 7 [22]. Due to the weak intermolecular forces of attraction between ZnO nanoparticles and PSf chains, ZnO nanoparticles will be directed under the active layer during membrane formation [59].

3.4. Characterization of membranes

3.4.1. Morphological properties

Pore size, pore size distribution, and cross-sectional structures of PVC and PSf based pristine and nanocomposite membranes were visualized by SEM in Figs 10 and 11 for PVC and PSf based membranes, respectively. Thickness value of each membrane was measured carefully from five different sections using image J software and average values are depicted in the figures. In addition,

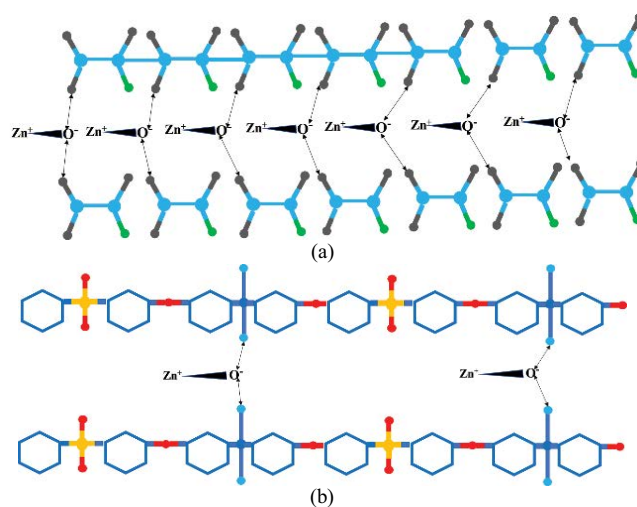


Fig. 9. Schematic view of the interaction of ZnO molecules with (a) PVC and (b) PSf polymer chains.

surface mean pore size of the fabricated membranes was analyzed using ImageJ software.

Fig. 10 shows that all the fabricated membranes exhibit a typical asymmetric porous microstructure with a dense skin layer supported by finger-like pores encompassing most of the volume on a porous substrate. For PVC nanocomposite membrane fabricated with 0.5% ZnO loading, the porosity and the mean pore size of the top layer was increased significantly and both connectivity and macro void volume of finger-like pores were enhanced in comparison to pristine PVC membrane, which plays an important role in improving membrane permeability (Figs. 10a–d). The pore-forming effect of ZnO nanoparticles was also confirmed by the surface mean pore size values highlighted in Fig. 10 along with porosity and overall mean pore size data given in Table 5. Hydrophilic structure of ZnO nanoparticles facilitates the phase inversion, that is, water penetrates the structure easily enhancing the exchange between solvent and non-solvent, which results in having a more porous top layer as well as improved finger-like structure [29,32]. When the ZnO loading was beyond 0.5% (1% and 2%), the surface porosity and the mean pore size decrease and become irregular, less uniform, and disorderly as also highlighted in Figs. 10e and g. Similar trend was also observed with the cross-section of the membrane, that is, the finger-like volume pores were obviously lower than that for 0.5% ZnO added membrane, which means that the desired morphology disappeared. This may be attributed to the increased viscosity of the casting solution delaying the exchange rate between solvent and nonsolvent.

The size and the distribution of the pores along with the pore connectivity through the cross-section of the pristine

PSf membranes were enhanced with 0.5% ZnO loading (Figs. 11a–h). The addition of hydrophilic ZnO to the pure membrane matrix caused a rapid exchange between solvent and water during the phase inversion. This has led nanocomposite membranes to have more developed morphological properties than pristine membranes [29,30]. However, when ZnO loading increased beyond 0.5%, the size of the surface pores became irregular, and the pore width and connectivity were reduced, which was due to the increase of the casting solution viscosity and delaying the exchange of solvent and nonsolvent, which subsequently resulted in a reduction of water flux [28,62].

Cross-section SEM images of pristine and nanocomposite membranes with 0.5 wt.% ZnO nanoparticle content were further analyzed in detail in terms of the finger-like pore width using ImageJ Software as illustrated in Fig. 12. The size distribution of finger-like pores in terms of pore width is increased from 0.5–3.0 μm to 3.0–7.0 μm for PVC based membranes whereas it increased from 1.0–4.5 μm to 2.0–5.5 μm for PSf based membranes with addition of 0.5% ZnO nanoparticles (Fig. 12). Effect of nanoparticle addition on the membrane formation is clearly observed in SEM images. Hydrophilic nanoparticles increased the exchange rate between solvent and nonsolvent which resulted in larger pore formation.

Morphological properties of PVC and PSf based pristine and nanocomposite membranes are given in Tables 5 and 6, respectively. As shown in Table 5, the porosity and average pore size of pristine PVC membranes increased up to 84.2% and 41.3 nm, respectively, with the addition of 0.5 wt.% ZnO to the casting solution. Addition of hydrophilic nanoparticles into casting solution facilitates the demixing process between solvent and nonsolvent which

Table 5
Morphological properties for PVC based pristine and nanocomposite membranes

| Membrane ID | ZnO/PVC (%, w/w) | Porosity (%) | Water uptake (%) | Thickness (μm) | Overall mean pore diameter (calculated from Eq. (11)) (nm) |
|--------------|---------------------|-----------------|---------------------|--------------------------------|---|
| Pristine PVC | 0 | 78.4 | 76.9 | 72 \pm 2 | 39.2 \pm 0.5 |
| PVC/0.25ZnO | 0.25 | 82.8 | 80.9 | 76 \pm 2 | 39.3 \pm 0.8 |
| PVC/0.50ZnO | 0.50 | 84.2 | 86.4 | 73 \pm 2 | 41.3 \pm 0.3 |
| PVC/0.75ZnO | 0.75 | 82.4 | 81.1 | 75 \pm 2 | 41.4 \pm 0.6 |
| PVC/1.00ZnO | 1.00 | 77.5 | 81.2 | 74 \pm 2 | 34.7 \pm 1.1 |
| PVC/2.00ZnO | 2.00 | 79.4 | 80.7 | 76 \pm 2 | 32.4 \pm 1.0 |

Table 6
Morphological properties for PSf based pristine and nanocomposite membranes

| Membrane ID | ZnO/PSf (%, w/w) | Porosity (%) | Water Uptake (%) | Thickness (μm) | Overall mean pore diameter (calculated from Eq. (11)) (nm) |
|--------------|---------------------|-----------------|---------------------|--------------------------------|---|
| Pristine PSf | 0 | 83.8 | 83.2 | 87 \pm 2 | 32.7 \pm 0.3 |
| PSf/0.10ZnO | 0.10 | 84.7 | 82.0 | 81 \pm 2 | 34.8 \pm 0.4 |
| PSf/0.25ZnO | 0.25 | 88.6 | 83.4 | 82 \pm 2 | 37.6 \pm 0.8 |
| PSf/0.50ZnO | 0.50 | 92.3 | 84.9 | 79 \pm 2 | 39.0 \pm 0.2 |
| PSf/0.75ZnO | 0.75 | 87.1 | 83.5 | 84 \pm 2 | 37.0 \pm 0.9 |
| PSf/1.00ZnO | 1.00 | 88.0 | 83.7 | 85 \pm 2 | 34.0 \pm 1.2 |

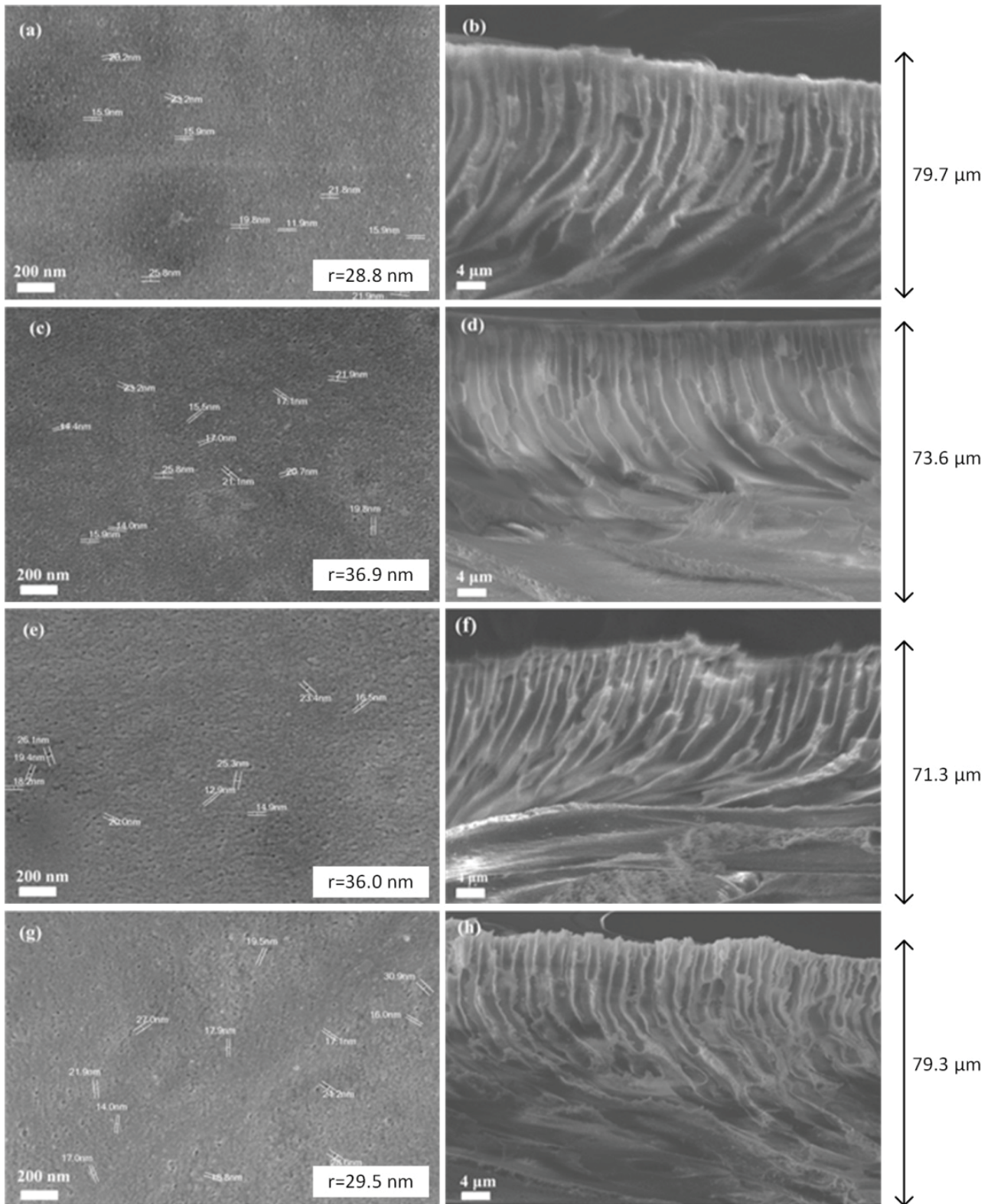


Fig. 11. Surface and cross-section images of PSf based membranes as a function of ZnO loading (a) surface image of pristine PSf membrane, (b) cross-section image of pristine PSf membrane, (c) surface image of PSf nanocomposite membrane with 0.5% ZnO loading, (d) cross-section image of PSf nanocomposite membrane with 0.5% ZnO loading, (e) surface image of PSf nanocomposite membrane with 0.75% ZnO loading, (f) cross-section image of PSf nanocomposite membrane with 0.75% ZnO loading, (g) surface image of PSf nanocomposite membrane with 1.0% ZnO loading, and (h) cross-section image of PSf nanocomposite membrane with 1.0% ZnO loading.

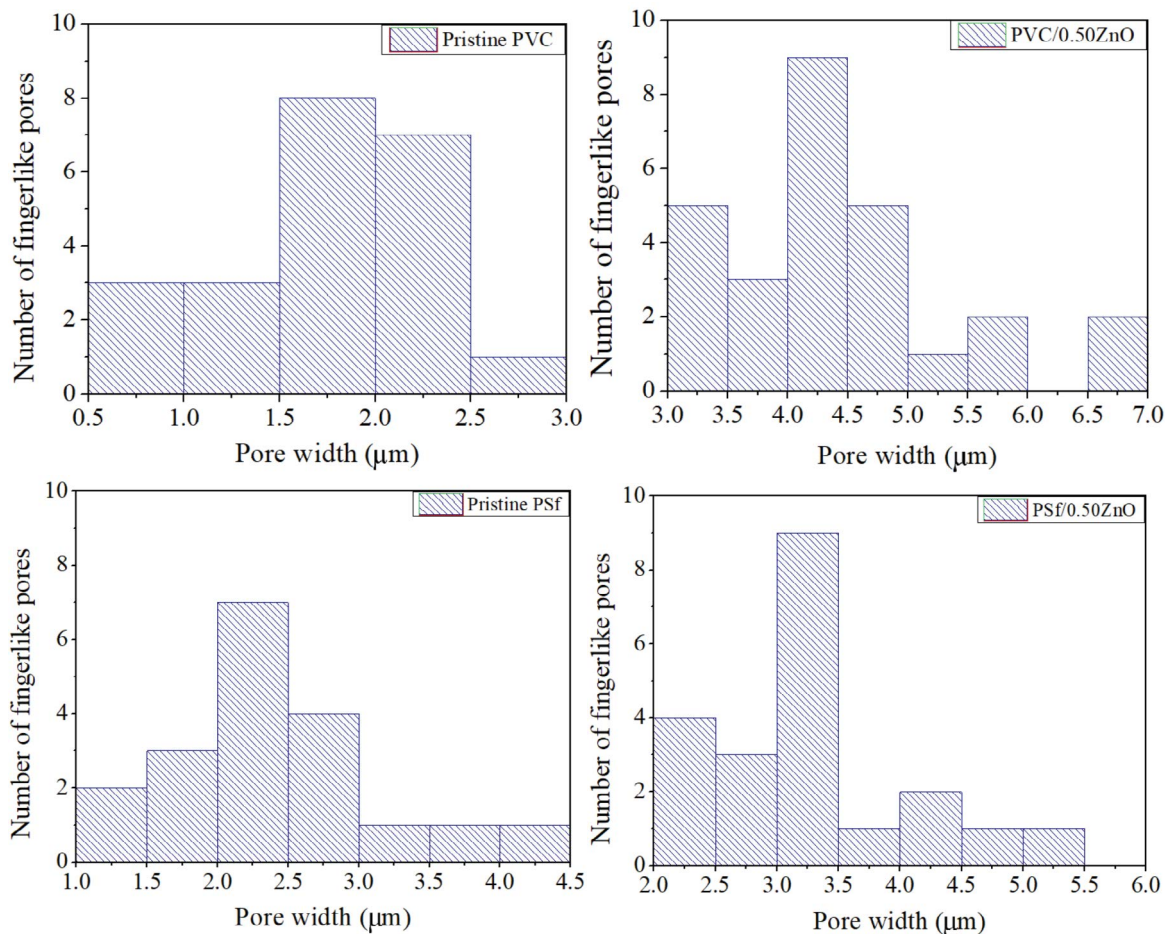


Fig. 12. Effect of ZnO addition on the size of finger-like pores (a) pristine PVC membrane, (b) PVC/0.50ZnO nanocomposite membrane, (c) pristine PSf membrane, and (d) PSf/0.50ZnO nanocomposite membrane.

in turn increases the transport of water into membrane matrix resulting in a higher porosity and surface pore size. Higher loadings of ZnO beyond 0.5 wt.% resulted in a reduction in porosity and mean pore diameter, which was probably due to the agglomeration of nanoparticles [12]. Furthermore, decrease of porosity and surface pore size can be attributed to the increase of the casting solution viscosity with higher nanoparticle loading which slows down the phase inversion process between solvent and nonsolvent. Such a trend was also observed in SEM surface and cross-section images and is in good agreement with flux values. For PSf based membranes, the porous structure and pore size were improved with the incorporation of ZnO particles into the membrane up to 0.5 wt.% loading level and tended to decrease with further addition, which can be attributed to pore blocking with a high concentration of ZnO nanoparticles. This was also visualized in the SEM images.

3.4.2. Water contact angle

Hydrophilicity of fabricated membranes were quantified using a water contact angle goniometer and the results are given in Fig. 13. The water contact angle of the pristine PVC

membrane was measured as 64.5° and gradually decreased with the addition of ZnO into the membrane matrix and reached the lowest value (38.5°) with 0.5 wt.% ZnO loading. Similarly, with the addition of hydrophilic ZnO nanoparticles into the PSf membrane matrix, the contact angle of pristine PSf membrane was reduced from 68.7° to 57° (Fig. 13a). This reduction in contact angle is due to the hydrophilicity of the ZnO nanoparticles as also observed by Alhashan et al. [39]. During the phase inversion, ZnO nanoparticles move toward the membrane surface to form a more hydrophilic surface. This change on the membrane surface results in a higher water flow through the membrane and hence a lower tendency to fouling which was supported by water flux and flux recovery ratio values (Figs. 3 and 6) [32]. The increasing tendency of contact angle values for both polymeric based membranes with higher loading levels of ZnO was due to the uneven distribution of nanoparticles over the surface of the membranes formed by the agglomeration of nanoparticles.

3.4.3. Thermo-chemical properties

Thermal stabilities of PVC and PSf based membranes were analyzed by thermogravimetric analysis as a function

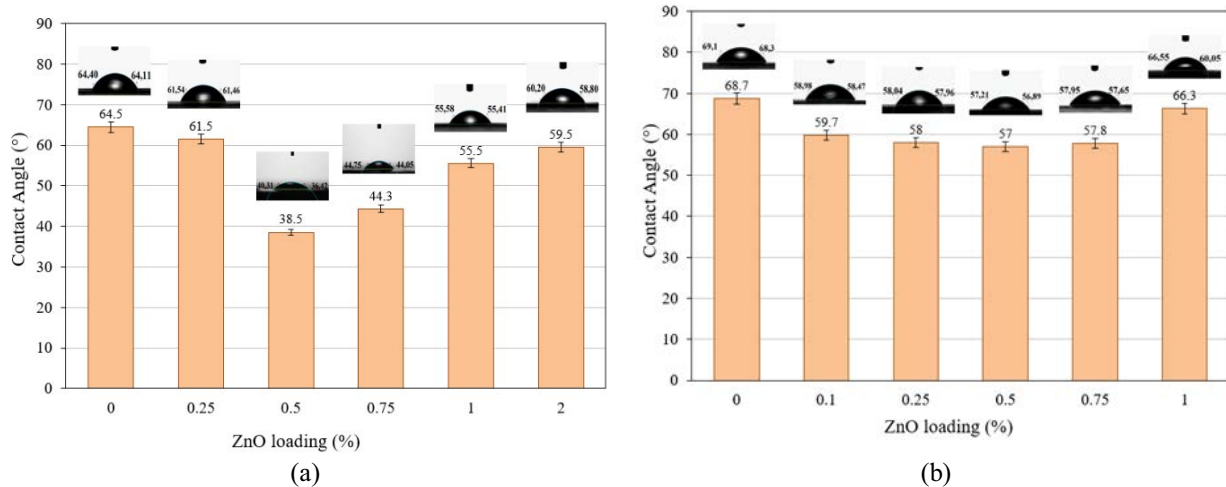


Fig. 13. Static water contact angle values of (a) PVC based and (b) PSf based membranes as a function of ZnO loading.

of ZnO loading (Fig. 14). As shown in Fig. 14a, the PVC polymer chains were degraded thermally between 203°C and 358°C, where the main weight loss (~60% weight loss) occurred for all membranes. The carbonization took place between 414°C to 501°C. The incorporation of ZnO into the membrane matrix disturbed the Van der Waals interaction between PVC chains, which resulted in a reduction of decomposition temperature from 241°C for pristine membranes to 203°C in the case of 2% ZnO loading and the nanocomposite membranes displayed lower weight loss compared to pristine PVC membrane [63]. As the ZnO ratio increased, the amount of remaining material increased from 9.6% to 24.7% (Fig. 14a) [6].

As shown in Fig. 14b, the PSf polymer chains in the PSf based membranes were degraded thermally between 381°C and 443°C, where the main weight loss (~60% weight loss) occurred. In the second decomposition temperature region (476°C–580°C) the material is carbonized [27]. For PSf based pristine and nanocomposite membranes, the change in thermal stability is not as significant as that of PVC based membranes. The addition of ZnO to the structure did not significantly affect the thermal properties of PSf based membranes. This is probably due to the weak bonding nature between the PSf polymer chain and ZnO as illustrated above in Fig. 9. As ZnO loading increased for nanocomposite PSf membranes, the amount of remaining material increased from 26.4% to 28.3%.

3.4.4. Mechanical properties

When a force is applied perpendicular to the surface of the membrane with repulsive force differential pressure, it is inevitable that deformation in the pore structure will occur after a certain time of exposure to this force. The mechanical strengths of the prepared PVC and PSf based pristine and ZnO doped nanocomposite membranes were determined by nanoindentation analysis based on Young's modulus and hardness values and the results are given in Fig. 15.

Young's modulus and hardness of pristine PVC membrane were found to be 8.9 and 2.7 MPa, respectively, and

those values gradually increased up to 113.7 and 5.3 MPa, respectively, with 0.5% ZnO loading and tended to decrease beyond further ZnO addition (Fig. 15a). For PSf based pristine membranes, Young's modulus and hardness values were found as 4.0 and 2.1 MPa, respectively, and increased with the addition of ZnO nanoparticles up to 0.75% loading reaching 139.6 and 10.0 MPa, respectively (Fig. 15b). The improvement in the mechanical properties may be associated with the interaction of nanoparticles with polymer chains. Further increase of ZnO amount in the casting solution inhibited the interaction between the polymer and the nanoparticles creating stress-convergence points, which resulted in a decrease of mechanical strength [22,64].

3.4.5. Crystal structure analysis of membranes

The XRD analysis was performed to determine the presence of ZnO nanoparticles in the membrane matrix. XRD patterns showing the crystal structures of pure ZnO nanoparticles, PVC based, and PSf based pristine and nanocomposite membranes are given in Fig. 16.

In Fig. 16a the clear peaks observed at $2\theta = 31.8^\circ, 34.5^\circ, 36.3^\circ, 47.5^\circ, \text{ and } 56.6^\circ$ are the characteristic peaks of ZnO nanoparticles representing a Wurtzite crystal structure. The non-sharp peaks seen in Fig. 16b at $2\theta = 16.5^\circ$ and 24.6° correspond to pristine PVC polymer. Weak peaks of pure ZnO are seen in the X-ray patterns of nanocomposite membranes containing a low percentage of ZnO. Peak intensity increased with increasing ZnO loading and peaks became apparent at 2% ZnO loading. This result indicates that the crystal structure of ZnO is not disturbed by the presence of PVC and can be successfully added to the membrane [65]. Fig. 16c indicates that PSf based membranes have a wide peak and amorphous structure in the X-ray diffraction pattern in the range of $2\theta = 17^\circ\text{--}30^\circ$ [66]. The decrease of the area under the peaks by the loading of ZnO nanoparticles to the PSf membrane matrix indicates the presence of ZnO in the structure. Significant peaks for ZnO nanoparticles could not be observed in the XRD pattern of PSf based nanocomposite membranes due to the weak interaction between PSf and ZnO nanoparticles [38].

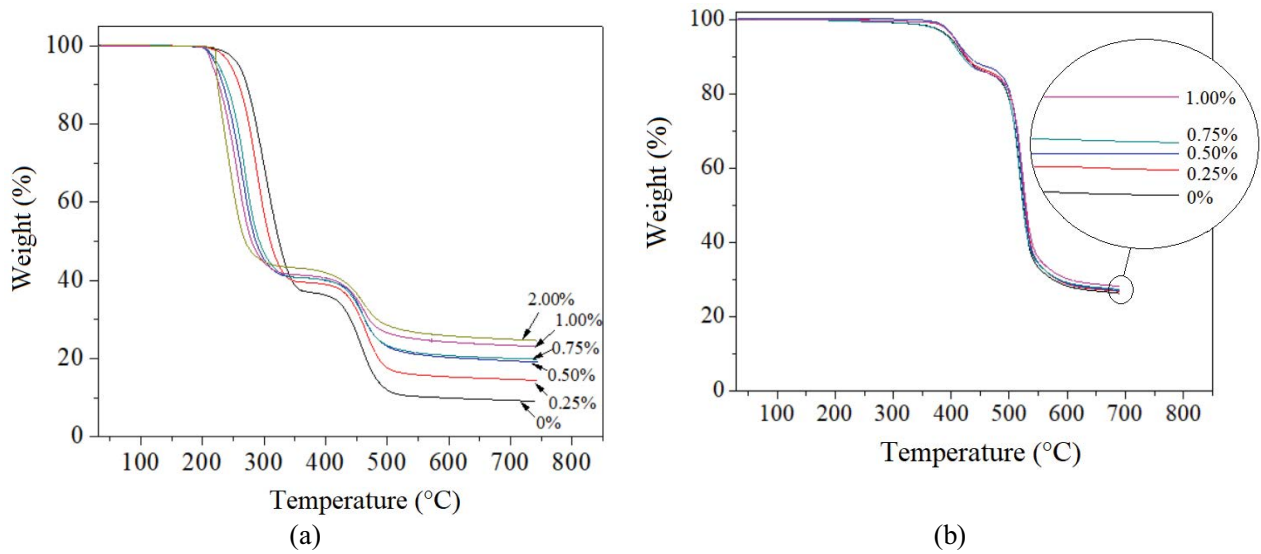


Fig. 14. Thermograms of (a) PVC and (b) PSf based pristine and nanocomposite membranes.

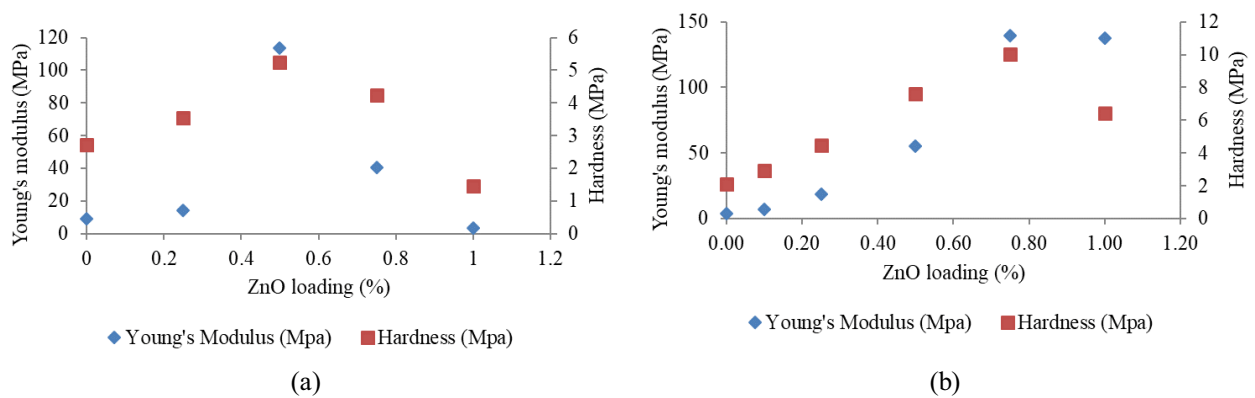


Fig. 15. Mechanical properties of (a) PVC and (b) PSf based pristine and nanocomposite membranes.

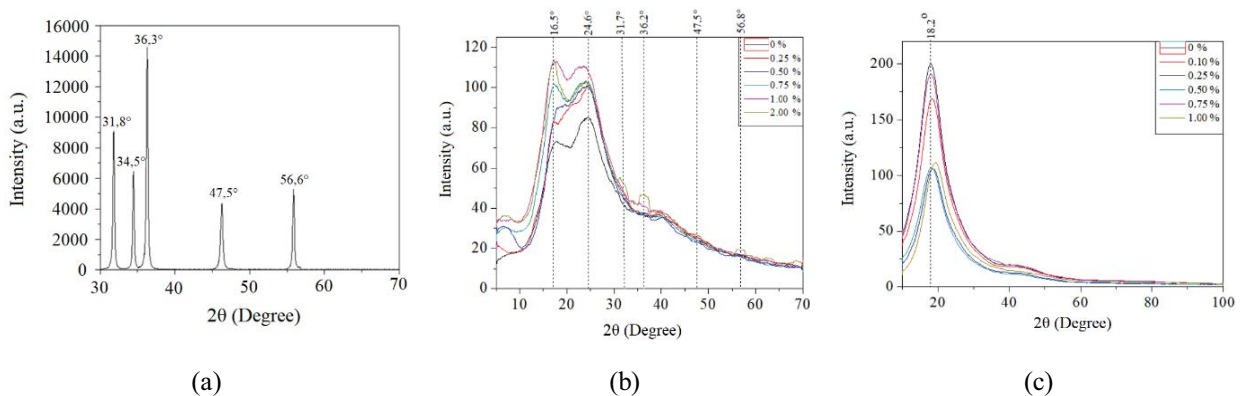


Fig. 16. X-ray diffraction patterns of (a) ZnO nanoparticles, (b) PVC based, and (c) PSf based pristine and nanocomposite membranes.

4. Conclusions

In the present study, filtration performance and characteristics of the nanocomposite membranes were investigated by the incorporation of ZnO nanoparticles into the

membrane matrix composed of PVC and PSf as polymeric backbone materials. Composition of casting solution has a significant impact on the filtration properties as well as morphology of membranes so before nanocomposite

membrane fabrication, polymer, and pore former concentrations of the casting solutions were investigated and the recipe which gave the best results was used in nanocomposite membrane fabrication. For PVC based pristine membranes, 18% polymer/solvent ratio with a PEG/PVC ratio of 1/3 yielded the best performance for flux (350 L/m²h) and SA rejection (93%), while for PSf based pristine membranes, 22% polymer/solvent ratio with a PEG/PSf ratio of 1/3 provided the most suitable flux performance (326 L/m²h) and SA rejection (90%). Incorporation of ZnO nanoparticles into the membrane matrices enhanced both PVC and PSf based membrane performance in terms of flux, rejection, and antifouling properties due to the alteration of the morphological structure. For PVC nanocomposite membranes, the highest water flux (420 L/m²h) and SA rejection (98%) were achieved with the addition of 0.5 wt.% ZnO. On the other hand, while the SA rejection has almost remained constant at about 90% with 0.5 wt.% ZnO addition, the water flux was increased by 23.5% (from 326 to 426 L/m²h) for PSf membranes. Although antifouling properties of PVC membranes have been successfully enhanced, those of PSf membranes could not be improved significantly as observed with flux recovery ratio test and resistance evaluation due to the fact that the interaction between PSf and ZnO is weaker than that between PVC and ZnO, which is attributed to the corresponding structure and the intermolecular forces between polymer and nanoparticle, which were also supported by the SEM images, water contact angle measurements, thermal, and mechanical properties. Finally, the results suggest that ZnO nanoparticles are more compatible with PVC than PSf polymer for the manufacturing of nanocomposite membranes in practice.

Acknowledgments

This study was supported by the Scientific and Technological Research Council of Turkey under the project number of 118M084.

References

- [1] M.S.S.A. Saraswathi, A. Nagendran, D. Rana, Tailored polymer nanocomposite membranes based on carbon, metal oxide and silicon nanomaterials: a review, *J. Mater. Chem. A*, 7 (2019) 8723–8745.
- [2] P.S. Goh, B.C. Ng, W.J. Lau, A.F. Ismail, Inorganic nanomaterials in polymeric ultrafiltration membranes for water treatment, *Sep. Purif. Rev.*, 44 (2015) 216–249.
- [3] M. Mulder, *Basic Principles of Membrane Technology*, 2nd ed., Springer Science & Business Media, Netherlands, 2012, pp. 124–138.
- [4] A.L. Ahmad, M. Sarif, S. Ismail, Development of an integrally skinned ultrafiltration membrane for wastewater treatment: effect of different formulations of PSf/NMP/PVP on flux and rejection, *Desalination*, 179 (2005) 257–263.
- [5] E. Arkhangelsky, A. Duek, V. Gitis, Maximal pore size in UF membranes, *J. Membr. Sci.*, 394 (2012) 89–97.
- [6] M. Pakbaz, Z. Maghsoud, Performance evaluation of polyvinylchloride/polyacrylonitrile ultrafiltration blend membrane, *Iran. Polym. J.*, 26 (2017) 833–849.
- [7] J. Zhang, M. Zhang, K. Zhang, Fabrication of poly (ether sulfone)/poly(zinc acrylate) ultrafiltration membrane with anti-biofouling properties, *J. Membr. Sci.*, 460 (2014) 18–24.
- [8] K.V. Peinemann, S.P. Nunes, *Membranes for Water Treatment*, John Wiley & Sons, Weinheim, Germany, 2010.
- [9] I.A. Ronova, S.V. Kryuchkova, M.Y. Yablokova, A.Y. Alentiev, L.G. Gasanova, M.I. Buzin, A.V. Kepman, Effect of polymers chemical structure on the membrane characteristics, *High Perform. Polym.*, 30 (2018) 58–66.
- [10] M. Asadinezhad, P. Lehocký, M. Mozeti Sáha, Recent progress in surface modification of polyvinyl chloride, *Materials*, 5 (2012) 2937–2959.
- [11] T.A. Saleh, V.K. Gupta, *Nanomaterial and Polymer Membranes: Synthesis, Characterization, and Applications*, Elsevier, Amsterdam, Netherlands, 2016.
- [12] J. Huang, K. Zhang, K. Wang, Z. Xie, B. Ladewig, H. Wang, Fabrication of polyethersulfone-mesoporous silica nanocomposite ultrafiltration membranes with antifouling properties, *J. Membr. Sci.*, 423 (2012) 362–370.
- [13] S. Ayyaru, Y.H. Ahn, Application of sulfonic acid group functionalized graphene oxide to improve hydrophilicity, permeability, and antifouling of PVDF nanocomposite ultrafiltration membranes, *J. Membr. Sci.*, 525 (2017) 210–219.
- [14] S. Liang, P. Gao, X. Gao, K. Xiao, X. Huang, Improved blending strategy for membrane modification by virtue of surface segregation using surface-tailored amphiphilic nanoparticles, *Front. Environ. Sci. Eng.*, 10 (2016) 113–121, doi: 10.1007/s11783-016-0875-5.
- [15] X. Cao, J. Ma, X. Shi, Z. Ren, Effect of TiO₂ nanoparticle size on the performance of PVDF membrane, *Appl. Surf. Sci.*, 253 (2006) 2003–2010.
- [16] S.J. Oh, N. Kim, Y.T. Lee, Preparation and characterization of PVDF/TiO₂ organic–inorganic composite membranes for fouling resistance improvement, *J. Membr. Sci.*, 345 (2009) 13–20.
- [17] J. Kim, B. Van der Bruggen, The use of nanoparticles in polymeric and ceramic membrane structures: review of manufacturing procedures and performance improvement for water treatment, *Environ. Pollut.*, 158 (2010) 2335–2349.
- [18] S.S. Madaeni, S. Zinadini, V.A. Vatanpour, New approach to improve antifouling property of PVDF membrane using *in situ* polymerization of PAA functionalized TiO₂ nanoparticles, *J. Membr. Sci.*, 380 (2011) 155–162.
- [19] Y. Wei, H.Q. Chu, B.Z. Dong, X. Li, S.J. Xia, Z.M. Qiang, Effect of TiO₂ nanowire addition on PVDF ultrafiltration membrane performance, *Desalination*, 272 (2011) 90–97.
- [20] H. Rabiee, M.H.D.A. Farahani, V.A. Vatanpour, Preparation and characterization of emulsion poly(vinyl chloride) (EPVC)/TiO₂ nanocomposite ultrafiltration membrane, *J. Membr. Sci.*, 472 (2014) 185–193.
- [21] G. Mishra, M. Mukhopadhyay, TiO₂ decorated functionalized halloysite nanotubes (TiO₂@HNTs) and photocatalytic PVC membranes synthesis, characterization and its application in water treatment, *Sci. Rep.*, 9 (2019) 4345, doi: 10.1038/s41598-019-40775-4.
- [22] L. Yan, Y.S. Li, C.B. Xiang, S. Xianda, Effect of nano-sized Al₂O₃-particle addition on PVDF ultrafiltration membrane performance, *J. Membr. Sci.*, 276 (2006) 162–167.
- [23] N. Maximous, G. Nakhla, W. Wan, K. Wong, Preparation, characterization and performance of Al₂O₃/PES membrane for wastewater filtration, *J. Membr. Sci.*, 341 (2009) 67–75.
- [24] T.A. Saleh, V.K. Gupta, Synthesis and characterization of alumina nano-particles polyamide membrane with enhanced flux rejection performance, *Sep. Purif. Technol.*, 89 (2012) 245–251.
- [25] D. Ghazanfari, D. Bastani, S.A. Mousavi, Preparation and characterization of poly(vinyl chloride) (PVC) based membrane for wastewater treatment, *J. Water Process Eng.*, 16 (2017) 98–107.
- [26] S. Balta, A. Sotto, P. Luis, L. Benea, B.V.D. Bruggen, J. Kim, A new outlook on membrane enhancement with nanoparticles: the alternative of ZnO, *J. Membr. Sci.*, 389 (2012) 155–161.
- [27] C.P. Leo, W.P.C. Lee, A.L. Ahmad, A.W. Mohammad, Poly-sulfone membranes blended with ZnO nanoparticles for reducing fouling by oleic acid, *Sep. Purif. Technol.*, 89 (2012) 51–56.
- [28] S. Liang, K. Xiao, Y. Mo, X. Huang, A novel ZnO nanoparticle blended polyvinylidene fluoride membrane for anti-irreversible fouling, *J. Membr. Sci.*, 394 (2012) 184–192.

- [29] H. Rabiee, V. Vatanpour, M.H.D.A. Farahani, H. Zarrabi, Improvement in flux and antifouling properties of PVC ultrafiltration membranes by incorporation of zinc oxide (ZnO) nanoparticles, *Sep. Purif. Technol.*, 156 (2015) 299–310.
- [30] S. Zhao, W. Yan, M. Shi, Z. Wang, J. Wang, S. Wang, Improving permeability and antifouling performance of polyethersulfone ultrafiltration membrane by incorporation of ZnO-DMF dispersion containing nano-ZnO and polyvinylpyrrolidone, *J. Membr. Sci.*, 478 (2015) 105–116.
- [31] A.L. Ahmad, J. Sugumar, N.F. Shoparwe, Antifouling properties of PES membranes by blending with ZnO nanoparticles and NMP-acetone mixture as solvent, *Membranes*, 8 (2018) 131–144.
- [32] Q.F. Alsahy, F.H. Al-Ani, A.E. Al-Najar, S.I. Jabuk, A study of the effect of embedding ZnO-NPs on PVC membrane performance use in actual hospital wastewater treatment by membrane bioreactor, *Chem. Eng. Process.*, 130 (2018) 262–274.
- [33] Z. Yu, X. Liu, F. Zhao, X. Liang, Y. Tian, Fabrication of a low-cost nano SiO₂/PVC composite ultrafiltration membrane and its antifouling performance, *J. Appl. Polym. Sci.*, 132 (2015) 41267, doi: 10.1002/app.41267.
- [34] W. Yu, L. Xu, N.Q. Graham, Contribution of Fe₃O₄ nanoparticles to the fouling of ultrafiltration with coagulation pre-treatment, *J. Sci. Rep.*, 5 (2015) 13067, doi: 10.1038/srep13067.
- [35] E. Demirel, B. Zhang, M. Papakyriakou, S. Xia, Y. Chen, Fe₂O₃ nanocomposite PVC membrane with enhanced properties and separation performance, *J. Membr. Sci.*, 529 (2017) 170–184.
- [36] N. Maximous, G. Nakhla, W. Wan, K. Wong, Performance of a novel ZrO₂/PES membrane for wastewater filtration, *J. Membr. Sci.*, 352 (2010) 222–230.
- [37] H.T. Dang, D. Rana, R.M. Narbaitz, T. Matsuura, Key factors affecting the manufacture of hydrophobic ultrafiltration membranes for surface water treatment, *J. Appl. Polym. Sci.*, 116 (2010) 2626–2637.
- [38] L. Shen, X. Bian, X. Lu, L. Shi, Z. Liu, L. Chen, K. Fan, Preparation and characterization of ZnO/polyethersulfone (PES) hybrid membranes, *Desalination*, 293 (2012) 21–29.
- [39] M. Alhoshan, J. Alam, L.A. Dass, N. Al Homaidi, Fabrication of polysulfone/ZnO membrane: influence of ZnO nanoparticles on membrane characteristics, *Adv. Polym., Technol.*, 32 (2013) 21369, doi: 10.1002/adv.21369.
- [40] J. Hong, Y. He, Effects of nano sized zinc oxide on the performance of PVDF microfiltration membranes, *Desalination*, 302 (2012) 71–79.
- [41] H. Rajabi, N. Ghaemi, S.S. Madaeni, P. Daraei, B. Astinchap, S. Zinadini, S.H. Razavizadeh, Nano-ZnO embedded mixed matrix polyethersulfone (PES) membrane: influence of nanofiller shape on characterization and fouling resistance, *Appl. Surf. Sci.*, 349 (2015) 66–77.
- [42] S. Javdaneh, M.R. Mehriani, M. Homayoonfal, Fabrication of polysulfone/zinc oxide nanocomposite membrane: investigation of pore forming agent on fouling behavior, *Korean J. Chem. Eng.*, 33 (2016) 3184–3193.
- [43] M.Z. Yunos, Z. Harun, H. Basri, M.F. Shohur, M.R. Jamalludin, S. Hassan, A.F. Ismail, Influence of inorganic additives on the performance of polysulfone ultrafiltration membrane, *J. Teknol.*, 65 (2013) 111–115.
- [44] B. Chakrabarty, A.K. Ghoshal, M.K. Purkait, Preparation, characterization and performance studies of polysulfone membranes using PVP as an additive, *J. Membr. Sci.*, 315 (2008) 36–47.
- [45] X. Zhang, Y. Wang, Y. Liu, J. Xu, Y. Han, X. Xu, Preparation, performances of PVDF/ZnO hybrid membranes and their applications in the removal of copper ions, *Appl. Surf. Sci.*, 316 (2014) 333–340.
- [46] S. Kang, A. Asatekin, A. Mayes, M. Elimelech, Protein antifouling mechanisms of PAN UF membranes incorporating PAN-g-PEO additive, *J. Membr. Sci.*, 296 (2007) 42–50.
- [47] B. Liu, C. Chen, T. Li, J. Crittenden, Y. Chen, High performance ultrafiltration membrane composed of PVDF blended with its derivative copolymer PVDF-g-PEGMA, *J. Membr. Sci.*, 445 (2013) 66–75.
- [48] E. Bazrafshan, H. Biglari, A.H. Mahvi, Humic acid removal from aqueous environments by electrocoagulation process using iron electrodes, *J. Chem.*, 9 (2012) 2453–2461.
- [49] L. Bai, H. Liang, J. Crittenden, F. Qu, A. Ding, J. Ma, G. Li, Surface modification of UF membranes with functionalized MWCNTs to control membrane fouling by NOM fractions, *J. Membr. Sci.*, 492 (2015) 400–411.
- [50] H. Zhao, S. Qiu, L. Wu, L. Zhang, H. Chen, C. Gao, Improving the performance of polyamide reverse osmosis membrane by incorporation of modified multi-walled carbon nanotubes, *J. Membr. Sci.*, 450 (2014) 249–256.
- [51] G. Wu, S. Gan, L. Cui, Y. Xu, Preparation and characterization of PES/TiO₂ composite membranes, *Appl. Surf. Sci.*, 254 (2008) 7080–7086.
- [52] P.T.P. Aryanti, R. Yustiana, R.E.D. Purnama, I.G. Wenten, Performance and characterization of PEG400 modified PVC ultrafiltration membrane, *Membr. Water Treat.*, 6 (2015) 379–392.
- [53] B. Ma, W. Xue, W. Li, C. Hu, H. Liu, J. Qu, Integrated Fe-based floc-membrane process for alleviating ultrafiltration membrane fouling by humic acid and reservoir water, *J. Membr. Sci.*, 563 (2018) 873–881.
- [54] J.H. Choi, J. Jegal, W.N. Kim, Fabrication and characterization of multi-walled carbon nanotubes/polymer blend membranes, *J. Membr. Sci.*, 284 (2006) 406–415.
- [55] Y. Yang, H. Zhang, P. Wang, Q. Zheng, J. Li, The influence of nano-sized TiO₂ fillers on the morphologies and properties of PSF UF membrane, *J. Membr. Sci.*, 288 (2007) 231–238.
- [56] Y. Orooji, M. Faghhi, A. Razmjou, J. Hou, P. Moazzam, N. Emami, W. Jin, Nanostructured mesoporous carbon polyethersulfone composite ultrafiltration membrane with significantly low protein adsorption and bacterial adhesion, *Carbon*, 111 (2017) 689–704.
- [57] C.W. Jung, H.J. Son, L.S. Kang, Effects of membrane material and pretreatment coagulation on membrane fouling: fouling mechanism and NOM removal, *Desalination*, 197 (2006) 154–164.
- [58] B.S. Lalia, V. Kochkodan, R. Hashaiekh, N. Hilal, A review on membrane fabrication: structure, properties and performance relationship, *Desalination*, 326 (2013) 77–95.
- [59] H.Y. Li, V. Chen, Chapter 10 – Membrane Fouling and Cleaning in Food and Bioprocessing, *Membrane Technology: A Practical Guide to Membrane Technology and Applications in Food and Bioprocessing*, Butterworth-Heinemann, Oxford, 2010, pp. 213–254.
- [60] S.J. Khan, N.P. Hankins, L. Shen, Submerged and Attached Growth Membrane Bioreactors and Forward Osmosis Membrane Bioreactors for Wastewater Treatment, N. Hankins, R. Singh, Eds., *Emerging Membrane Technology for Sustainable Water Treatment*, Elsevier, Boston, USA, 2016, pp. 277–296.
- [61] F. Liu, N.A. Hashim, Y. Liu, M.M. Abed, K. Li, Progress in the production and modification of PVDF membranes, *J. Membr. Sci.*, 375 (2011) 1–27.
- [62] A. Rahimpour, S.S. Madaeni, Improvement of performance and surface properties of nano-porous polyethersulfone (PES) membrane using hydrophilic monomers as additives in the casting solution, *J. Membr. Sci.*, 360 (2010) 371–379.
- [63] I.S. Elashmawi, N.A. Hakeem, L.K. Marei, F.F. Hanna, Structure and performance of ZnO/PVC nanocomposites, *Physica B*, 405 (2010) 4163–4169.
- [64] K. Wang, A.A. Abdalla, M.A. Khaleel, N. Hilal, M.K. Khraisheh, Mechanical properties of water desalination and wastewater treatment membranes, *Desalination*, 401 (2017) 190–205.
- [65] M. Radjabian, V. Abetz, Advanced porous polymer membranes from self-assembling block copolymers, *Prog. Polym. Sci.*, 102 (2020) 101219, doi: 10.1016/j.progpolymsci.2020.101219.
- [66] P.F. Andrade, A.F. Faria, S.R. Oliveira, M.A.Z. Arruda, G.M. Carmo, Improved antibacterial activity of nanofiltration polysulfone membranes modified with silver nanoparticles, *Water Res.*, 81 (2015) 333–342.